LIMNOLOGY
and
OCEANOGRAPHY: METHODS

Limnol. Oceanogr.: Methods 8, 2010, 539–551
© 2010, by the American Society of Limnology and Oceanography, Inc.

Toward continuous monitoring of seawater $^{13}CO_2/^{12}CO_2$ isotope ratio and pCO_2: Performance of cavity ringdown spectroscopy and gas matrix effects

Gernot Friedrichs[1], Julia Bock[1], Friedrich Temps[1], Peer Fietzek[2], Arne Körtzinger[2], and Douglas W. R. Wallace[2]*
[1]Institut für Physikalische Chemie, Olshausenstr. 40, Christian-Albrechts-Universität zu Kiel, 24098 Kiel, Germany
[2]Leibniz Institute of Marine Sciences, IFM-GEOMAR, Kiel, Germany

Abstract

The potential of a continuous wave cavity ringdown spectrometer for monitoring the isotope ratio $^{13}CO_2/^{12}CO_2$ and the partial pressure pCO_2 of CO_2 dissolved in water was thoroughly analyzed by quantitative measurements. Running calibration gas standards under typical operation conditions, a relative accuracy of $\Delta(\delta^{13}C[CO_2]) = \pm 0.1‰$ with 120 min averaging time has been demonstrated. Absolute uncertainties were determined to be $\Delta(\delta^{13}C[CO_2]) = \pm 0.2‰$ and $\Delta(xCO_2) = \pm 0.5$ ppmv. No principle problems were encountered when using the instrument in combination with a water-air equilibration setup. By contrast, when performing measurements of CO_2 in gas matrices with a composition different from that of ambient air, pressure broadening linewidth effects induced significant errors in both $\delta^{13}C(CO_2)$ and xCO_2 values. These effects, which compromise the accessible accuracy in environmental studies, can be quantitatively taken into account by using a spectroscopically based correction procedure. Relying on linewidth analysis, the instrument was shown to be capable of continuous and simultaneous measurement of $\delta^{13}C(CO_2)$, pCO_2, as well as water content and O_2 supersaturation, and thus holds the potential for online monitoring of these quantities aboard research vessels.

Due to the presence of anthropogenic CO_2 in the atmosphere, the world ocean acts as a net CO_2 sink, which is driven by the CO_2 partial pressure (pCO_2) difference across the air-sea interface. However, the global sink is masked by large regional and seasonal variations of surface water pCO_2 associated with natural physical and biological processes (Körtzinger et al. 2008; Watson et al. 2009). Through fractionation during photosynthesis, mixing, and the oceanic "Suess effect," all the mentioned processes alter the $\delta^{13}C$ value of surface water-dissolved inorganic carbon (DIC) (Zeebe and Wolf-Gladrow 2001; Emerson and Hedges 2008; Tagliabue and Bopp 2008). Here, the $^{13}C/^{12}C$ isotope ratio is expressed in terms of its $\delta^{13}C$ value in ‰

$$\delta^{13}C = \left(\frac{\left(^{13}C/^{12}C\right)_{sample}}{\left(^{13}C/^{12}C\right)_{V-PDB}} - 1 \right) \times 1000 \quad (1)$$

where $(^{13}C/^{12}C)_{V-PDB}$ refers to the isotopic composition of the Vienna Pee-Dee Belemnite reference standard.

Seasonal time-series data of DIC and its isotopic composition allow separation of the relative contributions of these processes to the surface layer carbon budget. The deconvolution of $\delta^{13}C$ and DIC changes has been demonstrated with data collected at the Hawaii and Bermuda Ocean Time-Series stations to address carbon dynamics operating in low-productivity subtropical gyres (Gruber et al. 2002; Quay and Stutsman 2003; Keeling et al. 2004). Comparable $\delta^{13}C$ time-series to examine seasonal carbon budgets in other parts of the ocean are scarce due to the difficulties of establishing regular long-term measurements of $\delta^{13}C$. For example, whereas Lüger et al. (2004, 2006) succeeded in regularly collecting data of pCO_2 and related properties in surface waters of the mid-latitude North Atlantic using autonomous water-air equilibra-

*Corresponding author: E-mail: friedrichs@phc.uni-kiel.de

Acknowledgments

We would like to thank CONTROS Systems & Solutions GmbH (Kiel, Germany) for the space and time rendering possible experiments with the water-air equilibrator setup. Many thanks go to Ingeborg Levin and Michael Sabasch (Institute of Environmental Physics, University of Heidelberg, Germany) for precise isotope ratio measurements on our compressed air samples, to Nils Andersen (Leibniz-Laboratory for Radiometric Dating and Stable Isotope Research, Kiel, Germany) for helpful discussions regarding technical pitfalls associated with isotope ratio measurements, to Meike Becker (Kiel University, Germany) for preliminary analysis of integrated line strength data, to Tobias Steinhoff (IFM-GEOMAR, Kiel, Germany) for the support of setting up the water-air equilibration system, and to Peter Croot and Andreas Oschlies for scientific advice. Financial support by the German Science Foundation (DFG - EC 80) in the framework of the cluster of excellence "The Future Ocean" is gratefully acknowledged.

DOI 10.4319/lom.2010.8.539

tor/non-dispersive infrared (NDIR) detection systems installed on a voluntary observing ship, discrete samples were collected for high-precision laboratory analysis of the $DI^{13}C/DI^{12}C$ ratio only on some crossings. Similarly, Quay et al. (2009) collected DIC samples on repeated container ship cruises across the subtropical and equatorial Pacific Ocean to estimate net community production rates from $\delta^{13}C$ air-sea disequilibrium. Reported spatial and temporal variabilities of oceanic $\delta^{13}C(DIC)$ in surface waters, which are directly related to $\delta^{13}C(CO_2)$, are in the range of several tenth of per mille. For example, averaged meridional changes across the Pacific and Atlantic basins are on the order of ~1‰ (Quay et al. 2007, 2009). Amplitudes of seasonal cycles measured at the subtropical time series stations near Hawaii (ALOHA, ~0.6‰) and Bermuda (BATS, ~0.2‰) are somewhat smaller (Gruber et al. 2002; Quay and Stutsman 2003). However, time and spatially resolved variations in biologically productive waters are expected to be more pronounced, but have not yet been fully characterized due the lack of online monitoring capabilities.

Isotope ratio mass spectrometry (IRMS) is the conventional method for measuring isotope ratios. It provides excellent absolute accuracies of measured $\delta^{13}C$ values, typically better than 0.05‰ with sample volumes as small as several milliliters of ocean water (deGroot 2004). Drawbacks of IRMS are (i) that the required collection, shipping, and processing of the samples is labor-intensive and costly and (ii) that the employed spectrometers cannot be operated in the field. In recent years, optically based instrumentation has emerged to provide alternative means for isotope ratio determination. These instruments are based on quantitative spectroscopic absorption techniques, where the ratio of the two isotopic species is determined by measuring separately the absorptions of $^{12}CO_2$ and $^{13}CO_2$ on vibrational transitions in the mid-infrared (mid-IR) or near infrared (near-IR) spectral range. Absorption cross sections of near-IR vibrational transitions (overtone and combination vibrations) are in general 10-100 times lower than in the mid-IR spectral range (fundamental vibrations). However, due to the availability of optical fiber technology and high quality near-IR diode lasers, comparable detection sensitivities have been reported for both mid-IR and near-IR based instruments. NDIR (Haisch et al. 1994; Jäger et al. 2005) and Fourier transform infrared (FTIR) spectrometers (Mohn et al. 2007) have been used as well as diode laser based instruments using modulation strategies (Castrillo et al. 2004; Lau et al. 2006). Cavity-enhanced detection schemes (Jost et al. 2006; Wahl et al. 2006) have been proven to provide outstanding detection sensitivity and reliability, and first commercial instruments based on wavelength scanned cavity ringdown spectroscopy (WS-CRDS) and off-axis integrated cavity output spectroscopy (OA-ICOS) have successfully entered the market. For a review of the large body of literature on optical isotope ratio spectroscopy, including selected applications, we refer to a review paper of Kerstel (2004) and the corresponding recent update given by Kerstel and Gianfrani (2008).

The usage of these new and cost-effective gas analyzers in field measurement campaigns has to be preceeded by comprehensive laboratory testing to assess spectrometer performance and reliability and to avoid and identify possible pitfalls. Moreover, in the light of the expected natural variations in $\delta^{13}C$ outlined above, it has to be verified that the short- and long-term precision requirements of ~0.2‰ and ~0.05‰, respectively, can be met. In this work, we have coupled a CO_2 isotopic gas analyzer with a conventional water-air equilibrator setup similar to the equilibrator systems used aboard research vessels. Step experiments for pH have been performed to assess the spectrometer $\delta^{13}C$ response to changes in pCO_2. In addition, the influence of variable gas matrices, which could possibly compromise the use of the spectrometer for surface ocean CO_2 analysis at variable saturation levels of oxygen, was studied in detail.

Cavity ringdown spectroscopy—Cavity ringdown spectroscopy (CRDS) is an ultrasensitive absorption based detection method with many applications in physical and analytical chemistry. The absorption coefficient α of a species is determined by measuring the rate of absorption of light circulating in a high finesse optical cavity. Figure 1 illustrates the schematic setup of a CRDS experiment. In conventional CRDS, a short pulse of laser light is injected into a stable optical cavity formed by two (or more) highly reflective mirrors. The light is repeatedly reflected back and forth between the mirrors and the small amount of light leaking through the exit mirror is monitored by a photodetector. The time constant of the exponential decrease of the light intensity in the cavity, the so-called ringdown, is determined by the light losses originating from residual mirror transmission, absorption of the sample, and (interfering) scattering processes. In the absence of additional wavelength-dependent losses, the ringdown equation

$$\alpha = \frac{1}{c}\left(\frac{1}{\tau_r} - \frac{1}{\tau_r^0}\right) \qquad (2)$$

holds, where τ_r^0 and τ_r are the reciprocal ringdown time constants of the empty cavity and a cavity containing the absorber, respectively, and c is the speed of light. Pulsed CRDS has been successfully used for gas phase spectroscopy (Berden et al. 2000), quantitative detection of weakly absorbing or low concentration gas phase species (McIlroy and Jeffries 2002), and rate constant measurements based on time-resolved detection schemes (Friedrichs 2008). Minimum detectable absorptions of $\alpha_{min} = 1\times10^{-8}$ cm^{-1} are readily achievable. A fur-

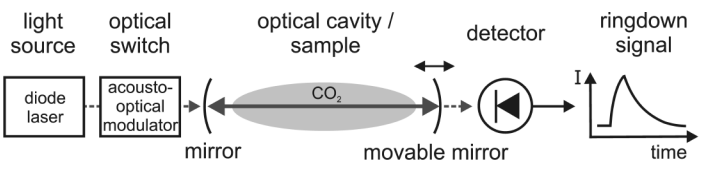

Fig. 1. Schematic setup of a *cw*-CRDS spectrometer.

ther increase in sensitivity is obtained when using narrow bandwidth continuous wave (*cw*) lasers. In *cw*-CRDS, matching of the narrow bandwidth detection laser output to the resonance frequency comb structure of the high-finesse optical cavity is critical. Hence the exit mirror of the ringdown cavity is typically piezo-tuned (*see* Fig. 1), until light starts to build up in a single resonant cavity mode. Having reached a preset light level, a fast optical switch (e.g., an acousto-optical modulator) is used to turn off the light source and the subsequent ringdown event can be observed (Romanini et al. 1997). As a result of the single cavity mode excitation and an increased data accumulation frequency (typically >100 measurements per second), *cw*-CRDS offers a higher sensitivity on the order of $\alpha_{min} \approx 1\times10^{-9}$ cm^{-1} (Mazurenka et al. 2005) Merging the advantages of sensitivity, high spectral resolution and direct absorption, *cw*-CRDS is ideally suited to measure concentrations of trace gas species by monitoring individual rovibrational absorption lines. Typically, a distortion-free absorption line profile is obtained by scanning the laser frequency over the absorption feature of interest. After baseline subtraction, which is necessary to account for the empty cavity losses ($1/\tau_r^0$ in Eq. 2), integrated absorption line strengths can be directly determined from the measured CRD spectrum—in principle without the need for calibration. $\delta^{13}C(CO_2)$ values are simply extracted from the measured ratio of the absorption of individual $^{12}CO_2$ and $^{13}CO_2$ lines. In this work, $x(^{13}CO_2)$, $x(^{12}CO_2)$, and $\delta^{13}C$ of CO_2 dissolved in water were measured following equilibration with air at a known pressure. The determined xCO_2 values were converted to their respective values for dry air by taking into account the volumetric effect of water vapor, which was known from simultaneous measurement of xH_2O. Assuming ideal gas behavior, the determined CO_2 mole fraction can be used as a direct measure of the pCO_2 value as well.

Materials and procedures

cw-CRDS isotopic analyzer—A commercial *cw*-CRD spectrometer (EnviroSense 2050, Picarro) capable of performing $^{12}CO_2$, $^{13}CO_2$, and water vapor concentration measurements was used in all experiments. Briefly, a tunable *cw* distributed feedback diode laser centered at an emission wavelength around 1600 nm was coupled into a V-shaped, piezo-tuned ringdown cavity. A continuous gas flow of about 20 sccm (standard cm^3/min) was pumped through the cavity with an inner volume of approximately 33 cm^3 at a pressure of 186.6 mbar and a temperature of 45.0°C. $^{12}CO_2$ was detected at the R(36)(30013 ← 00001) transition (AFGL notation: $\nu_1\nu_2 l\nu_3 n$. Strongly coupled Fermi-resonances are not assigned explicitly but the respective vibrational modes are numerated (n) starting with the energetically highest band) at a wavenumber of 6251.76 cm^{-1}, $^{13}CO_2$ at the R(12)(30012 ← 00001) transition at 6251.32 cm^{-1}, and H_2O at the (040,5,5,0 ← 000,6,6,1) transition (notation $\nu_1\ \nu_2\ \nu_3, J, K_A, K_C$) at 6250.42 cm^{-1}(Mikhailenko et al. 2008; Perevalov et al. 2008a, 2008b). An etalon-based wavelength monitor, which was actively locked to known wavelengths by a spectral feedback algorithm, ensured fast and symmetrical sampling of the individual absorption lines. A rather coarse scan increment of 0.02 cm^{-1} was chosen to sample the line profiles. The spectra were fitted with a multi-order fitting routine assuming Galatry line profiles with line parameters valid for ambient air. Galatry line profiles, next to Doppler and pressure broadening, also take into account the collisional Dicke narrowing effect (Galatry 1961). The three Galatry model parameters are the Doppler width, which is a known quantity at a given temperature, the collisional broadening parameter y, which is proportional to the total pressure, and the narrowing parameter z. To constrain the fit, in the fitting routine, a preset ratio $y/z = 0.3215$ was used, thus leaving the collisional broadening parameter y the sole adjustable parameter. Instead of the integral absorption, the resulting peak heights were taken as a measure of the respective concentrations to minimize possible errors arising from residual baseline fitting issues. Finally, the measured $^{13}CO_2/^{12}CO_2$ ratio was converted to $\delta^{13}C(CO_2)$ values based on a calibration polynomial. As will be explained and investigated in more detail in the Section "Gas Matrix Effects," this data reduction procedure bears the risk of yielding erroneous results when using gas matrices different from ambient air.

Raw data points were created every 6-11 s based on individual measurements of several hundred ringdown events. According to manufacturer specification, which is subject to verification in this study, the stated precision of the instrument was 0.3‰ for $\delta^{13}C$ (5 min average) and 50 ppbv for xCO_2 (1 min average) at ambient CO_2 concentration levels. Predrying of the samples was not obligatory as the instrument corrects for water vapor influences based on the simultaneously measured H_2O mole fraction.

Water-air equilibrator—Water-air equilibration experiments were performed using a commercial showerhead equilibration system (Model 8050, General Oceanics, water flow: 3 L/min, equilibrator volume: ~0.5 L) equipped with an NDIR CO_2 gas analyzer (Li-COR, LI-6262). Including the errors arising from instrumental drift and calibration accuracy, the NDIR gas analyzer readout was accurate to within ±3 ppmv. The analyzer was calibrated every 8 h using gas standards and was operated at very low sample gas humidity using a Nafion dryer (Perma Pure, <0.1% H_2O by volume) to avoid any water absorption interference. The *cw*-CRDS analyzer was supplied with predried sample gas (~1% H_2O, thermoelectrically cooled condenser) using a bypass flow line. The analyzed gas was returned to the headspace of the equilibrator. The water-air equilibration system was connected to a thermostatted 130 L water tank filled with de-ionized water. A carbonate system was prepared by adding controlled amounts of sodium bicarbonate and sodium carbonate (DIC ≈ 2.6 mmol/kg). However, due to the unknown CO_2 content of the de-ionized water, it was not possible to adjust the system to a specific target pCO_2 with high precision. Moreover, due to the inevitable need for pressure compensation, the partly

open system slowly equilibrated with ambient air CO_2. Abrupt changes in water pH and pCO_2 were generated by injections of 0.1 M solutions of sodium hydroxide or 0.5 M hydrochloric acid.

Gas mixtures—Experiments on the effect of variable gas matrices were performed by diluting compressed air samples with known amounts of N_2 (99.999%), O_2 (99.995%), Ar (99.998%), and He (99.999%) using a flow system with calibrated mass flow controllers (Aera, FC series). Depending on the particular gas mixture, the relative error of CO_2 content can be estimated to be 1% to 2%. As trace amounts of CO_2 with unknown $\delta^{13}C(CO_2)$ value would have had interfered with the isotope ratio measurements, added gases were checked to contain negligible amounts of CO_2. A small correction was applied for O_2 gas, which was found to be contaminated with ~2 ppm of CO_2. Finally, gas samples with variable water content were prepared by mixing a flow of dry air with a flow of humid air that had passed through a bubble saturator filled with water beforehand.

Assessment

Analyzer performance—Several tests were carried out to assess the response time, stability, precision, and accuracy of the *cw*-CRDS isotopic analyzer. First of all, compressed air and/or nitrogen gas cylinders were connected to the analyzer using stainless steel tubing and an optional particle filter (MicraTube MTA, <0.05μm, MicraFilter), which was installed directly before the gas inlet. Note that additional gas filters were installed inside the analyzer to protect the optical cavity (Teflon filters, Mykrolis) such that the instrument could be operated without external filtering as well. The response time of the analyzer was determined from the measured CO_2 mole fractions following fast switching between the two gas supplies using magnetic valves. As expected, due to adsorption effects induced by the particle filters and due to the slow flow rate through the instrument (20 sccm), rather long response times on the order of 400 s (90% value) were observed. However, using a bypass flow of 100 sccm or removal of the optional particle filter decreased the response time to 85 s, which is in good agreement with the technical specifications and fast enough for most environmental monitoring applications.

Figure 2 displays the results of an experiment using two different compressed air cylinders with slightly different CO_2 content and $\delta^{13}C$ value. Whereas the upper two traces seem to reveal a consistent switching behavior for $^{12}CO_2$ and $^{13}CO_2$, the lower trace clearly indicates small differences resulting in distinct switching spikes visible in the measured $\delta^{13}C$ values. With a duration of merely ≈3 min, these switching spikes do not seriously interfere with the measurements. They were present in all our experiments and are possibly due to intrinsic instrumental effect, such as the baseline or absorption line-locking algorithm of the instrument, the disturbance of the established adsorption equilibria at the tubing and detection cell walls, or a combination of both. Measurements with and without an additional particle filter as well as observed tendencies of spike sizes in switching experiments using gas mixtures with different CO_2 contents and isotopic compositions lead us to the conclusion that adsorption/desorption effects are at least partly responsible for the observed effects. A simple molecular picture of the adsorption/desorption process can be drawn that is consistent with the monitored sign of the spikes. On the one hand, it is feasible that a change to overall lower gas phase CO_2 concentration leads to a net desorption of CO_2 molecules, which can be assumed to be faster for the lighter isotope yielding a negative transient $\delta^{13}C$ signal. On the other hand, an increased CO_2 concentration leads to a net adsorption of CO_2. Again, this process can be assumed to be faster for the light isotope because of its higher translational velocity and thus would result in a positive $\delta^{13}C$ bias.

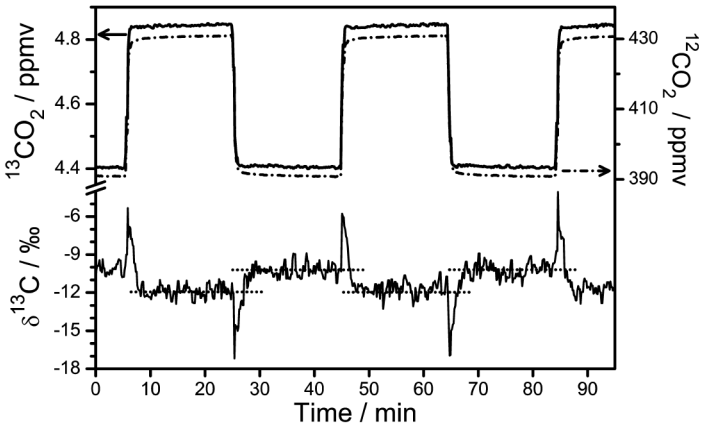

Fig. 2. Typical *cw*-CRDS CO_2 isotopic analyzer output. $^{12}CO_2$ (upper solid curve), $^{13}CO_2$ (dash-dotted curve), and $\delta^{13}C$ (lower solid curve) traces as monitored during a switching experiment between two different compressed air gas samples.

The precision of the instrument was checked and precision enhancement strategies were verified based on an Allan deviation plot analysis. The Allan (or two-sample) variance is defined as the time average of the sample variance of m adjacent averages, $A_s(\tau)$ and $A_{s+1}(\tau)$, of $k \times m$ time series data points x

$$\sigma^2_{\text{Allan}}(\tau) = \frac{1}{2(m-1)} \sum_{s=1}^{m-1} \left[A_{(s+1)}(\tau) - A_s(\tau) \right]^2 \qquad (3)$$

with

$$A_s(\tau) = \frac{1}{k} \sum_{l=1}^{k} x_{(s-1)k+l} \;, \; s = 1,\ldots,m \qquad (4)$$

where $\tau = k \times \Delta t$ corresponds to the integration time of the samples (average of k data points with a time interval of Δt). Hence the Allan deviation σ_{Allan} represents the precision of the instrument with respect to an immediately repeated experiment with raw data averaging over k data points.

Figure 3 illustrates a modified Allan plot analysis, where the Allan deviation (noisy black curve) is plotted versus the averaging time τ in double logarithmic scale. As expected for random noise, for short averaging times (i.e., <100 min), the Allan deviation improves according to a $1/\sqrt{\tau}$ law (dashed line). At long averaging times, non-statistical noise (e.g., drift components) start to prevail resulting in an optimum Allan deviation of 0.08‰ at τ = 130 min. Note that the experiment was performed with a compressed air gas sample at ambient CO_2 level and a better precision can be expected for higher concentration CO_2 mixtures. Interestingly, in most experiments, a resonance-like feature of unknown source was observed for long averaging times (τ ≈ 900 min for the experiment shown in Fig. 3), pointing out an oscillatory baseline behavior of the instrument. At even longer averaging times, the Allan deviation started to decrease again indicating an excellent long-term stability of the instrument. In agreement with independent, repeated analyses of calibration gas standards performed within 1 y of operation without recalibration of the instrument, the long-term stability of the instrument was found to be about 0.15‰. To assess the accuracy of a time-series experiment, this value of $\delta^{13}C$ long-term repeatability has to be taken into account. In Fig. 3, the gray curve illustrates the "idealized" accuracy, i.e., the accuracy of the instrument excluding a possible additional absolute calibration offset error. This curve was obtained by adding a feasible correction to the continuously averaged Allan standard deviation data. Here, a simple linear correction term was assumed, which was (i) set to 0.15‰ at τ = 10 min (the shortest feasible averaging interval) and (ii) linearly decreased with time to a value of zero at τ ≈ 800 min (the maximum of the Allan deviation curve). The flat progression of the resulting gray curve implies that extended averaging does, in fact, not satisfactorily enhance the performance of the instrument with respect to absolute $\delta^{13}C$ measurements.

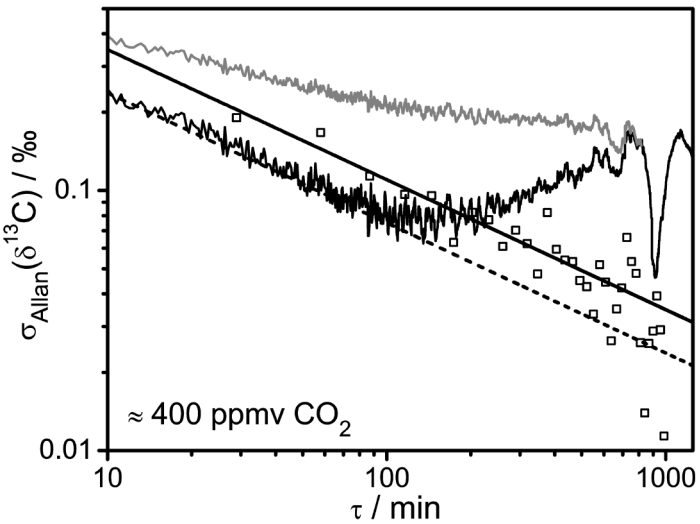

Fig. 3. Modified Allan plot analysis. The noisy black solid curve and the dashed line represent the Allan deviation of a continuous averaging experiment and the respective ideal statistics behavior. The gray curve corresponds to the (idealized) accuracy including a correction for the long-term stability of the instrument (*see* text). The squares and the solid line represent the accuracy of an alternative reference approach based on periodically switching between the sample and a reference or working gas standard with known $\delta^{13}C$ value.

Of course, remaining long-term drift issues can be easily overcome by performing measurements relative to a reference gas standard. Such a measurement was simulated by periodically switching between two different compressed air samples. Switching spikes were cut out of the data trace and the Allan deviation was calculated from the measured $\delta^{13}C$ differences between the two gas mixtures. Corresponding data points for an experiment with 20 min switching interval, which are shown in Fig. 3 as squares, reveal that it is in fact possible to reduce the long-term drift components. The data points follow the straight line determined by the random noise of the measurements (solid line in Fig. 3). Assuming a reference gas standard with known $\delta^{13}C$ value, this line represents the attainable accuracy of the instrument, which is 0.1‰ at τ = 120 min and 0.05‰ at τ = 480 min, thus close to the accuracy of a typical IRMS experiment.

A comparison of the optimum statistical noise reduction of the simple averaging (dashed line in Fig. 3) and reference approach (solid line) reveals an offset of the reference measurements toward lower precision. This is not unexpected since in the case of the switching experiment both the unknown gas sample and the reference mixture are measured only half of the time. Therefore, the attainable precision can be expected to be roughly a factor of $\sqrt{2}$ lower, which is in good agreement with the experimental offset. Consequently, a further improvement of the sensitivity of the reference approach can be expected when operating two (or more) isotopic analyzers in parallel. Moreover, to ensure highest performance, the switching interval should be set short enough to escape from long-term drift components but also long enough to avoid unwanted data loss by the inevitable need for cutting-off switching spikes. As noticeable deviations from the random noise behavior are observed for averaging times τ >100 min, switching intervals as long as 50 min should provide a natural choice for our instrument.

Finally, the absolute accuracy of the precalibrated instrument was tested by running working gas standards, which were characterized by IRMS ($\delta^{13}C$, ±0.05‰) and high precision gas chromatography (xCO_2, ±0.3 ppmv). From three independent measurements, systematic offsets ($\delta^{13}C_{measured} - \delta^{13}C_{standard}$) = 2.8(2)‰ (at xCO_2 = 380 ppmv) and ($xCO_{2measured} - xCO_{2standard}$) = 2.7(5) ppmv were determined. Moreover, by running gas standards with elevated CO_2 mole fractions (350 ppmv < xCO_2 < 1000 ppmv), the determined $\delta^{13}C$ values were checked to be independent of xCO_2. Unexpectedly, in contrast to specifications ($\Delta[\delta^{13}C] < 0.03$‰ per 100 ppmv change in xCO_2), a significant divergence of $\Delta(\delta^{13}C) \approx 0.38$‰ per 100 ppmv CO_2 was found and was taken into account in all following measurements based on a second-order calibration

polynomial. These significant deviations from factory pre-calibration point out the well-known importance of double checking calibration data. Nevertheless, all measurements were within the long-term stability limits of 0.15‰ for $\delta^{13}C$ and 0.16 ppmv for xCO_2 as they were derived from Allan analyses. No systematic drift of the calibrated offset values were noticed over a time period of 1 y, and relative readouts for gas mixtures with different $\delta^{13}C$ but constant xCO_2 were found to be reliable without further correction.

Water-air equilibration experiment—The applicability of *cw*-CRDS to monitor pCO_2 and $\delta^{13}C$ of CO_2 dissolved in water was tested by combining the isotopic analyzer with the water-air equilibration setup. pH-step experiments were performed to induce a strong perturbance of the water phase carbonate equilibria resulting in a pronounced change of the pCO_2 value, which was followed by measuring the gas phase mole fraction $xCO_2(g)$ and $\delta^{13}C(CO_2[g])$ value. Figure 4 displays the outcome of such a pH-step experiment using a carbonate system of salinity $S \approx 0.1$ at 25°C. Starting at $xCO_2(g) \approx 700$ ppm, the addition of NaOH or HCl induced significant CO_2 mole fraction changes on the order of 250 ppm. In contrast, the equilibrium values of $\delta^{13}C$ remained essentially unchanged within the scatter of the data. Again, the signal exhibited strong switching spikes. The purpose of this experiment was 3-fold: (i) to rule out potential pitfalls that may prevent the use of the instrument in combination with a commercial equilibrator system (e.g., pressure balance problems), (ii) to check the reliability of the instrument under experimental conditions close to the conditions expected in surface ocean CO_2 field measurements, and (iii) to check linearity and accuracy of the determined parameters by intercomparison with a conventional NDIR pCO_2 system.

With a time constant of merely 2 min, which includes the mixing within the 130 L water tank, the water-air equilibration, and the gas exchange in the *cw*-CRDS analyzer, the response time of the equilibrator setup was found to be short. Running the NDIR CO_2 sensor in parallel with the *cw*-CRDS showed that both the observed response times as well as the measured absolute CO_2 levels agreed well within the error limits of the two different analyzers. No problems were met when operating the *cw*-CRDS in combination with the water-air equilibrator, showing the potential of *cw*-CRDS to reliably measure $xCO_2(g)$ and hence pCO_2 values without a need for frequent calibration or a requirement of drying sample gas streams.

Next to changes in pCO_2, altering the pH affects the abundance of the different carbon species present in the water-carbonate system and thus results in equilibrium fractionation of the different isotopic species as well. According to well-known fractionation factors (Mook 1986; Zhang et al. 1995), changing the pH from a very low pH value, where most of the DIC exists as dissolved CO_2, to pH ≈ 8 (free scale), where most of the carbon is found as HCO_3^-, a relative change of $\Delta(\delta^{13}C[CO_2]) = -8.8‰$ and –10.1‰ is expected for temperatures of 25°C and 15°C, respectively. In good agreement with these numbers, we actually found a systematic shift of $\Delta(\delta^{13}C\{CO_2[g]\}) \approx -1.0‰$ when lowering the experimental temperature from 25°C to 15°C. Also in agreement with the experiment, for the small pH-step induced in the measurements shown in Fig. 4, a barely detectable isotopic shift (<0.05‰) was expected to occur.

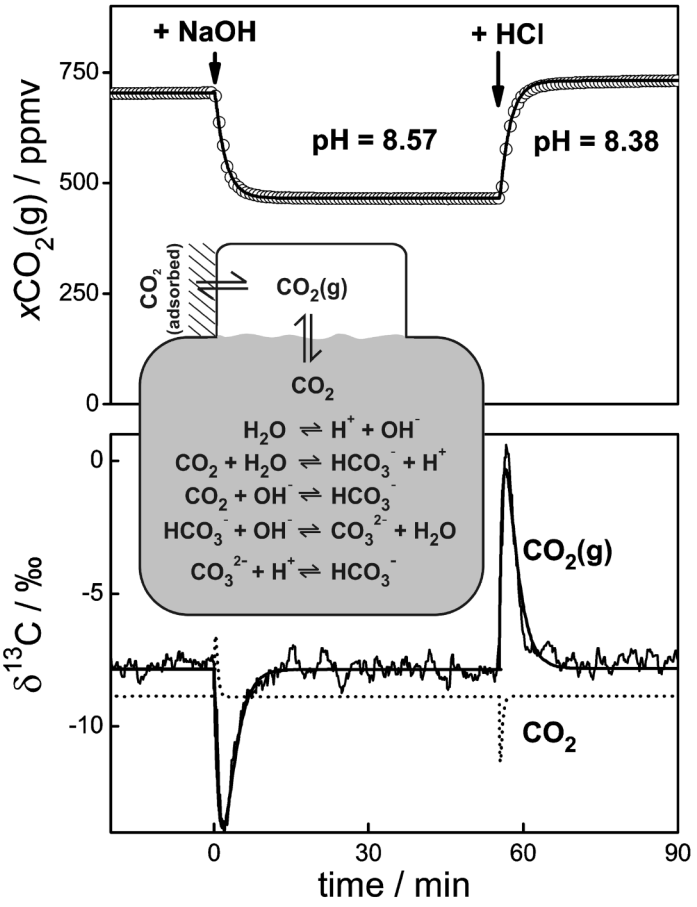

Fig. 4. Measured time series of xCO_2 and $\delta^{13}C$ during a water-air equilibration experiment. Solid and dashed curves are the results of a simulation, which is based on the box model illustrated in the insert. Note that the experimental $\delta^{13}C$ values have been arbitrarily offset by +11.5‰ to fit the model entry, which was set to $\delta^{13}C(DIC) = 0‰$.

To further specify the response of the experimental setup, a full kinetic simulation of the experiment has been performed. Simulation results, which are based on the box model outlined in the insert of Fig. 4, are shown as solid and dashed curves. Model input parameters such as reaction rate constants, kinetic fractionation factors, and equilibrium constants, which were needed to assure proper sets of forward and reverse reaction rate constants, were taken from the compilations given by Zeebe and Wolf-Gladrow (2001). The switching spikes visible in the $\delta^{13}C$ signal were approximated by assuming an adsorption/desorption effect of CO_2 at the cell and tubing walls. As the objective of this study was to test the feasi-

bility of water-air equilibration experiments rather than a kinetic analysis of isotopic equilibria, only the most important details of the simulations will be outlined here. Also note that we could as well have assumed a slow instrumental $\delta^{13}C$ signal response instead of an adsorption/desorption effect without changing the outcome of the simulation.

Briefly, initial parameters of the carbonate system were obtained from the dissolved carbonate/bicarbonate quantities (DIC ≈ 2.6 mmol/kg) and the measured pCO_2 value. The size of the CO_2 adsorption effect was estimated based on the height of the obtained $\delta^{13}C$ signal spikes following injections of known amounts of NaOH or HCl. Relying on these assumptions, it was possible to nicely reproduce both the $xCO_2(g)$ and $\delta^{13}C(CO_2[g])$ signals as indicated by the solid curves in Fig. 4. Clearly, in agreement with findings of Zeebe et al. (1999), liquid phase equilibria were found to equilibrate rapidly (discernible as short spikes in $\delta^{13}C$ signal of dissolved CO_2, dashed curve) whereas the observed experimental response time of several minutes was dominated by the relaxation of the water-air and adsorption equilibria (discernible as rather slow adjustment of the $xCO_2(g)$ signal and the long $\delta^{13}C(CO_2[g])$ spikes, solid curves).

Gas matrix effects—The applied fitting procedure of the $^{13}CO_2$ and $^{12}CO_2$ absorption lines is based on peak heights instead of using peak integrals. Although yielding more stable fitting results and thus increasing the precision of the instrument, this approach takes the risk of yielding erroneous results. When using gas matrices different from the composition of ambient air, different y and z Galatry line profile parameters arise. These account for collisional line broadening and Dicke narrowing effects and may be different for the analyzed $^{12}CO_2$ and $^{13}CO_2$ absorption lines, respectively. Therefore, systematic offsets in the calculated $\delta^{13}C(CO_2)$ and inaccurate pCO_2 values can be expected to occur for gas matrices different from air.

Figure 5 summarizes experimentally observed $\delta^{13}C$ offsets (open circles) measured for compressed air gas samples diluted with different amounts of N_2, O_2, Ar, and He. The leftmost four data points were taken for different air samples, where the first data point was measured with pure air as a reference and the next three points were obtained by using synthetic air samples that were prepared by mixing gas flows of air, O_2, and N_2. The scatter of these three points reflects the accuracy of the gas mixture preparation procedure. The insert of Fig. 5 illustrates part of the original data, where the dashed line indicates the actual $\delta^{13}C$ value measured for the pure air sample. Clearly, changing the gas matrix results in an immediate response of the instrument with respect to the $\delta^{13}C$ output. Huge positive (He, N_2) and negative (Ar, O_2) biases up to a value of +58‰ for the addition of 51% He have been observed. Measurements were also performed with samples containing different amounts of water vapor yielding a 3.84‰ offset per 1% water content. Obviously, measured $\delta^{13}C$ values need to be corrected for this pronounced gas matrix effect to ensure reliable isotope ratio measurements. In the following, a straightforward data treatment procedure that is based on spectroscopic reasoning will be presented in detail. As can be seen from the corrected data points drawn as solid circles in Fig. 5, this procedure efficiently accounts for the observed gas matrix induced offsets.

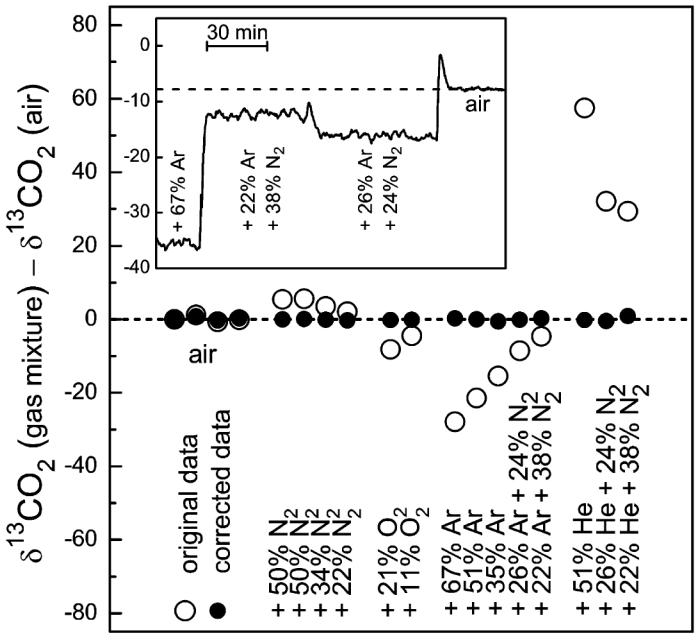

Fig. 5. Measured $\delta^{13}C(CO_2)$ values for different gas matrices. The actual $^{13}CO_2/^{12}CO_2$ isotope ratio remained constant for all mixtures. Gas matrix composition are denoted in terms of excess mole fractions relative to the composition of ambient air (eg, +50% N_2 corresponds to a gas matrix composition of $x_{Air} = 0.50$ and $x_{N_2}^{excess} = 0.50$).

Effect on measured CO_2 mole fractions—A smaller but significant gas matrix effect has been observed for the CO_2 concentration signal as well. For example, in comparison with the mole fraction calculated from the mixing ratio of Ar and air, a 11% too high absolute $^{12}CO_2$ mole fraction was measured by the instrument for a 65% Ar mixture. As the CO_2 is calculated from the peak height of the measured $^{12}CO_2$ absorption line, the overestimated CO_2 value is in line with the expected smaller collisional broadening of Ar compared to air. Precise pressure broadening coefficients for the (30013 ← 00001) band of CO_2 have been measured recently by Nakamichi et al. (2006). Broadening coefficients, which were analyzed assuming Voigt line shape profiles, were found to decrease both as a function of temperature and rotational excitation. The pressure broadening coefficients as derived from the data given by Nakamichi et al. (2006) for our experimental conditions are summarized for the R(36) $^{12}CO_2$ rotational transition in Table 1. Here, the pressure broadening of air was calculated according to

$$\Delta\tilde{\nu}_L = \sum_i x_i \Delta\tilde{\nu}_{L,i} \quad (5)$$

Table 1. Doppler ($\Delta\tilde{\nu}_D$) and pressure ($\Delta\tilde{\nu}_L$) broadening (FWHM, in units of cm^{-1}) of the R(36) $^{12}CO_2$ and R(12) $^{13}CO_2$ absorption lines at T = 45°C and p = 186.6 mbar. Pressure broadening was estimated from the data given by Nakamichi et al. (2006). The last two columns compare experimental gas matrix offset factors φ with a prediction based on calculated Voigt profile heights.

	$^{12}CO_2$			$^{13}CO_2$				
Gas	$\Delta\tilde{\nu}_D$	$\Delta\tilde{\nu}_I$	$\Delta\tilde{\nu}_L / \Delta\tilde{\nu}_L^{air}$	$\Delta\tilde{\nu}_D$	$\Delta\tilde{\nu}_L$	$\Delta\tilde{\nu}_L / \Delta\tilde{\nu}_L^{air}$	$\left(\frac{h_{L,13}}{h_{L,12}} \times \frac{h_{L,12}^{air}}{h_{L,13}^{air}} - 1\right)$/‰	φ/‰
N_2	0.01204	0.02459	1.0475	0.01191	0.02830	1.0391	5.1	10.9
O_2		0.01956	0.8333		0.02353	0.8638	–20.1	–38.7
Ar		0.01823	0.7763		0.02206	0.8101	–21.1	–41.9
He		0.01986	0.8461		0.02059	0.7559	96.6	113
H_2O								386
Air		0.02348	1		0.02723	1	0	0

where the x_i correspond to the mole fractions of N_2, O_2, and Ar of ambient air. It is close to the value of N_2 and it is roughly twice as large as the Doppler broadening $\Delta\tilde{\nu}_D$.

To check the assumption that a variable pressure broadening is the dominating cause of the observed variations in the measured $^{12}CO_2$ concentrations when using different gas matrices, calculated Voigt profile peak heights are compared to measured $^{12}CO_2$ concentrations in Figure 6. Here, the former was normalized with respect to the corresponding peak height in air and the latter with respect to the actual $^{12}CO_2$ concentration calculated from the mixing ratio of the different gas streams. In this way, the dashed line in Fig. 6 corresponds to a one-to-one correlation between the $^{12}CO_2$ concentration mismatch and the pressure-broadening effect. Within the scatter of the data, where the error bars indicate the uncertainty of the calculated $^{12}CO_2$ concentration arising from the mixing procedure, indeed a good agreement between predictions and measurements has been found. Next to minor uncertainties of the reported pressure broadening coefficients, remaining discrepancies may be due to small systematic shifts going along with the baseline fitting procedure under different gas matrix regimes. Note that for the used experimental conditions, the description of the line profiles by either Voigt or Galatry profiles is expected to be of minor importance. Of course, pressure-broadening coefficients obtained for Voigt and Galatry fitting are somewhat different and care should be taken to use a consistent set of parameters.

Predicted $\delta^{13}C$ offset based on linewidth data—Being confident that the observed $\delta^{13}C$ offsets can be essentially traced back to line shape effects, the pressure broadening data in Table 1 were used to predict the magnitudes of the required $\delta^{13}C$ offset corrections. For this purpose, the pressure broadening coefficients of the the (30012 ← 00001) band of $^{13}CO_2$ were assumed to be the same as for the (30013 ← 00001) $^{12}CO_2$ band measured by Nakamichi et al. (2006). Nevertheless, significant deviations of the pressure-broadening coefficients arise for the absorption lines of the two isotopic species, which have been detected at transitions corresponding to different rotational excitation. However, the small differences between the observed changes for the $^{12}CO_2$ and $^{13}CO_2$ lines and not the resulting absolute change of the line center absorptions are important for isotope ratio measurements. These relative changes have been calculated assuming Voigt absorption line profiles and are given in the fourth column of Table 1. In qualitative agreement with the experiments shown in Fig. 5, a small positive bias is predicted for N_2. In contrast, medium-sized negative biases are determined for O_2 and Ar and a large positive offset of 96.6‰ for pure He. Both size and sign of the required gas matrix offset correction were found to be very sensitive to minor variations in the used pressure broadening coefficients of the different sample gases relative to air.

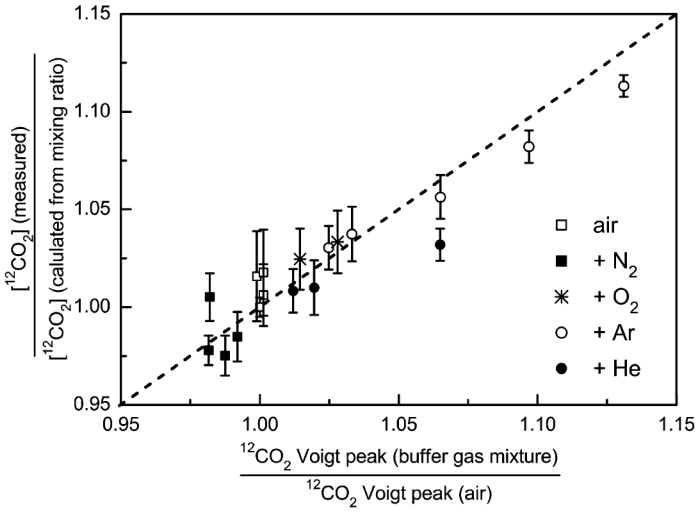

Fig. 6. Relative $^{12}CO_2$ concentration mismatch measured for different gas matrices in comparison with Voigt profile peak height ratios calculated using literature values for the respective pressure broadening coefficients. The dashed line corresponds to a perfect correlation between the two quantities.

Experimental determination of linear gas matrix correction factors—The resulting combined pressure broadening of a given

gas mixture is determined by a weighted sum over its components according to Eq. 5. In contrast, the total linewidth resulting from the convolution of Doppler and pressure broadening and the corresponding peak height is a more complicated function of the pressure broadening but can be approximated by polynomial expressions. However, as differences between the pressure broadening of the different gases are small under the experimental conditions used in this work (Table 1), a linear approximation should hold and hence a linear dependence of the $\delta^{13}C$ offset according to

$$\Delta(\delta^{13}C) = \sum_i x_i \varphi_i \tag{6}$$

can be hoped for as well. Here, the φ_i represent the respective gas matrix offset factors. For example, a value of $\varphi_{Ar} = -10‰$ would correspond to a –10‰ underestimated $\delta^{13}C$ value measured by the instrument when replacing pure air by pure Ar.

In Fig. 7, the assumed linear dependence of the pressure broadening upon mixture composition is verified by plotting the experimentally determined Galatry line shape parameter y as function of the mixture composition. Linear correlations were found in all cases. The thick dashed line marks the experimental value of dry air, $y = 1.5778$, and thus intersects the linear fits of the O_2, N_2, Ar, and He data at the respective mole fractions found in dry air. Note that y is related to the pressure broadening $\Delta\tilde{\nu}_L$ according to

$$y = \frac{\Delta\tilde{\nu}_L}{\Delta\tilde{\nu}_D} \times \sqrt{\ln 2} \tag{7}$$

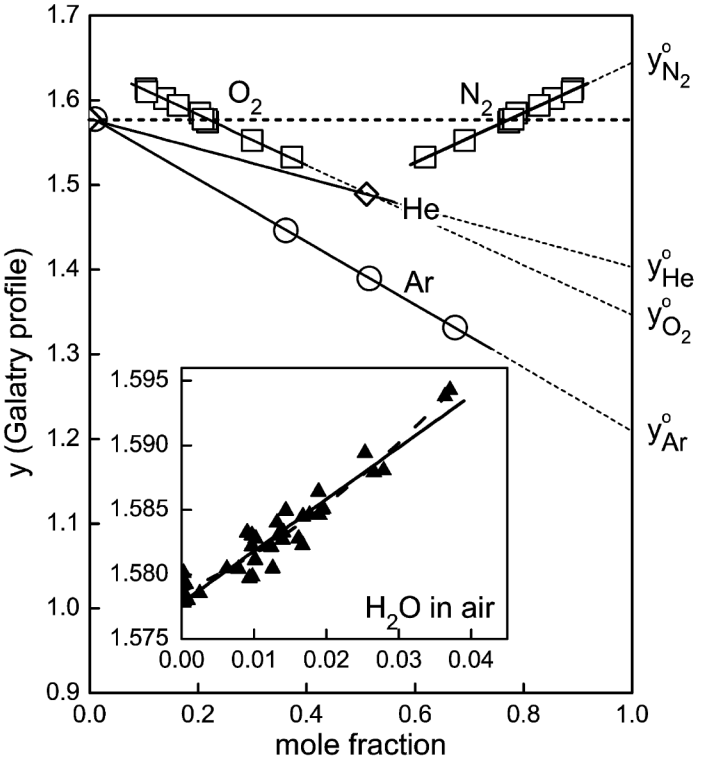

Fig. 7. Pressure broadening of the $^{12}CO_2$ absorption line in terms of the Galatry line profile parameter y determined by the internal fit procedure of the isotopic analyzer. Linear trends have been observed for all gas mixtures components.

Deduced Galatry linewidths (FWHM) are only 3% to 7% lower than those calculated from the Voigt parameters given in Table 1, showing that there is reasonable agreement with the pressure broadening data reported by Nakamichi et al. (2006).

Finally, the insert of Fig. 7 illustrates the results obtained for humid air. Data were obtained from free running experiments measuring ambient laboratory air as well as from experiments with distinct relative humidities (RH) generated by mixing dry air (0% RH) with air saturated with water (100% RH). Whereas a second-order polynomial seems to be a slightly better representation in case of H_2O (dashed curve), again a straight line fit is sufficient to approximate the data.

Having set the framework for a linear correction procedure, optimum gas matrix offset factors were found by fitting the φ_i parameters in Eq. 6 to minimize the observed $\delta^{13}C$ deviations of the experiments outlined in Fig. 5. Of course, $\Delta(\delta^{13}C) = 0‰$ holds for dry air such that the parameter set can be easily checked for consistency. The determined φ_i values are given in the fifth column of Table 1 and can be compared with the predictions based on the literature data (fourth column). Both the size and sign of the experimentally determined and theoretically predicted offset corrections are in very good agreement indeed. Small adjustments of the pressure broadening parameters on the order of ±5% are sufficient to explain the remaining deviations. However, minor baseline fitting issues or limitations of the used line shape model partly account for the remaining minor discrepancies as well. Therefore, instead of relying on linewidth data taken from the literature, an experimental determination of the offset factors as demonstrated in this section should always be preferred.

O_2 saturation determination from measured linewidths—Knowing the linewidth response of the instrument with respect to the four principal components of air, it is possible to calculate the Galatry line shape parameter according to

$$y = \sum_i x_i y_i^{\circ} \tag{8}$$

where y_i° corresponds to the value of y determined for the pure component i. For example, $y_{O_2}^{\circ} = 1.34393$ was obtained from the linear fit of the corresponding O_2 data shown in Fig. 7. As the instrument measures the mole fraction of water independently, it is possible to calculate the O_2 mole fraction from the experimentally measured Galatry y parameter. A detailed conversion procedure is outlined in the Appendix, which is based on the assumption that equilibrated ocean water/gas phase samples are characterized by the same Ar/N_2 ratio as it is found for ambient air. Note that trace gases such as CO_2, CH_4, and N_2O exert minor linewidth effects and hence can be

neglected in these calculations. The procedure was found to be accurate within $\Delta xO_2 \approx \pm 0.005$ allowing us to measure the relative saturation level of oxygen in water without the need for an additional oxygen sensor.

Discussion

The performance of the instrument was tested based on a measurement scheme with periodic switching between a test sample and a reference sample with known $\delta^{13}C$ value. In these experiments, a relative accuracy of $\Delta(\delta^{13}C) = \pm 0.1‰$ with 120 min averaging time and ±0.05‰ with 480 min averaging time was achieved. Running working gas standards, the absolute uncertainty of the measured $\delta^{13}C(CO_2)$ value has been determined to be ±0.2‰. Similarly, an absolute uncertainty of the determined CO_2 mole fraction of $\Delta(xCO_2) = \pm 0.5$ ppmv has been determined. The instrument has been found to yield stable output over 1 y of operation such that frequent re-calibration of the instrument is not necessary. This is in contrast with IRMS- or NDIR-based detection schemes, where the absolute accuracy strongly relies on frequent referencing. Note that the switching scheme used in our $\delta^{13}C$ measurements was only needed to overcome a periodic long-term oscillation of the $\delta^{13}C$ value on the order of 0.15‰. Running working gas standards is dispensable, however, if a lower precision is sufficient. For example, short-term fluctuations of $\delta^{13}C$ in ocean dissolved CO_2 are expected to exceed 0.15‰ significantly.

No principle problems were encountered when using the instrument in combination with a water-air equilibrator setup. Of course, the usual requirements with respect to equilibrator temperature and pressure stability need to be met to ensure reliable data. Whereas a change of the equilibration temperature of 1°C significantly affects the equilibrated pCO_2 value (~4.3%), the temperature sensitivity of the determined $\delta^{13}C$ value is rather small (~0.12‰) (Mook et al. 1974; Takahashi et al. 1993).

The accuracy of the instrument is little affected by the presence of water vapor because the water content of the sample is measured continuously. The determined $\delta^{13}C$ and xCO_2 values can thus be corrected for linewidth or volumetric effects online. Simple predrying by using thermo-electrical coolers to prevent water condensation inside the flow system or the spectrometer was found to be sufficient.

It generally turned out that linewidth effects have to be properly taken into account to correct for systematic offsets caused by alterations of the gas matrix. The required corrections set a limit to the accessible precision in water-air equilibration experiments. It is well known that the ocean water saturation state can be significantly different from equilibrium with the atmosphere. For example, as a result of biological activity, oxygen is typically found to be supersaturated by 0.5% to 1.5% relative to the saturation level of N_2 and Ar in surface waters of the subtropical North Pacific Ocean (Hamme and Emerson 2006). Similarly, upwelled sub-surface waters from oxygen minimum zones can be strongly oxygen deficient. In high productivity waters or during phytoplancton blooms much higher supersaturation levels of >15% are regularly observed (Kuss et al. 2006; Körtzinger et al. 2008). Due to physical processes, N_2 and Ar are typically enriched in surface waters as well, but follow similar seasonal trends such that the Ar/N_2 ratio can be assumed as a fixed quantity. In Table 2, expected $\delta^{13}C$ offsets and relative xCO_2 deviations are given for a set of gas matrices. Calculations are based on the linear correction procedure given by Eq. 6 for $\delta^{13}C$ and on line shape calculations using reported Galatry line shape parameters for xCO_2. Using synthetic air (air without Ar) instead of dry ambient air makes necessary a $\delta^{13}C$ correction of + 0.43‰. Such a correction is already significantly higher than the accuracy of the instrument. Using humid air with 1% water content also significantly shifts the $\delta^{13}C$ value by 3.86‰. Four more realistic scenarios with elevated O_2 contents have been considered in Table 2. Clearly, with deviations of $\delta^{13}C$ up to 2‰, for accurate measurements the O_2 content has to be known. Here, the scenario with the relative supersaturation parameter $s = 0.024$ (corresponding to an oxygen content of $xO_2 = 21.29\%$ instead of 20.90% in pure air) reflects the accuracy of the approximate O_2 concentration determination procedure outlined in the Appendix. Therefore, without an additional oxygen sensor, the accuracy of the instrument in water-air equilibration experiments is limited to >0.2‰. Of course, better accuracy can be readily achieved by measuring the O_2 content separately by using, for example, calibrated oxygen optodes (Tengberg et al. 2006).

As can be seen from the relative xCO_2 deviations given in Table 2, corresponding gas matrix corrections are needed for

Table 2. Predicted $\delta^{13}C$ offsets and relative xCO_2 deviations for different gas matrix scenarios. *s* denotes the relative oxygen supersaturation parameter as it is defined in the Appendix.

				High O_2 air			
	Air	Synthetic air	Humid air	$s = 0.25$	$s = 0.25$	$s = 0.125$	$s = 0.024$
xN_2	0.7810	0.7889	0.7732	0.7422	0.7348	0.7611	0.77710
xO_2	0.2090	0.2111	0.2069	0.2483	0.2458	0.2291	0.21294
xAr	0.0100		0.0099	0.0095	0.0094	0.0098	0.00995
xH_2O			0.0100		0.0100		
$(\Sigma x_i \varphi_i)$/‰	0	0.43	3.86	–1.92	1.96	–0.98	–0.19
xCO_2(measured)/xCO_2	1.0000	0.9982	0.9980	1.0058	1.0037	1.0030	1.0006

xCO_2 as well. Overall, the effect can be accounted for in a straightforward manner and the estimated additional uncertainty of 0.6‰, corresponding to $\Delta(xCO_2)$ = 0.24 ppmv at xCO_2 = 400 ppmv, is rather small.

An alternative way for an experimental determination of the gas matrix effect could have been based on an intentional, alternating dilution of the sample gas mixture with a CO_2-free reference mixture with known gas matrix composition. Owing to the linear gas matrix offset behavior outlined in Eq. 6, it should be possible to directly infer the gas matrix effect from the measured difference between the $\delta^{13}C(CO_2)$ values with and without gas matrix dilution. For example, when using a dilution flow of 50% standard ambient air ($\delta^{13}C$ offset = 0), the measured $\delta^{13}C$ difference would account for half of the actual $\delta^{13}C$ offset of the sample gas mixture. Of course, such a procedure relies on very accurately measured $\delta^{13}C$ values such that long-term drift components of the instrument may compromise the required long averaging times. Furthermore, utmost care should be taken in such an approach to assure the purity of the dilution flow, because small CO_2 impurities with unknown $\delta^{13}C$ value can significantly affect the measured $\delta^{13}C$ difference. Moreover, in view of the small gas matrix effects observed for xCO_2, a very accurate measurement of the sample and dilution mass flow would be needed to perform a similar correction for the xCO_2 value.

In principle, the necessary correction procedures could have been completely avoided by using a detection scheme that is based on integrated instead of line center absorptions. However, especially in isotope ratio measurements, residual baseline fitting inaccuracies may introduce significant errors in integration-based detection schemes as well. In a preliminary analysis, integrated absorptions have been calculated for the same data set as the one used for determining the gas matrix offset factors (Fig. 5). Relying on the measured Galatry line shape parameters y for each single data point, it was in fact possible to largely correct the observed $\delta^{13}C$ offsets. However, the scatter of the data increased by a factor of 5, and even after integration significant offsets on the order of 1.5‰ remained. These would have to be still corrected based on a separate calibration procedure.

Indeed, the need for accurately measured empty cavity ringdown times that resemble the baseline of the CRD spectrum is a weak point of CRDS and other cavity-enhanced absorption techniques. As demonstrated in this work, however, the high sensitivity and reproducibility of the measurements supersedes this drawback by far. Moreover, as *cw*-CRDS constitutes essentially a simple narrow bandwidth absorption experiment, the outlined linear correction procedure could be based on strict spectroscopic reasoning without the need for obscure calibration corrections.

Conclusion

cw-CRDS is a reliable, absolute detection technique that enables simultaneous measurement of $\delta^{13}C$ and pCO_2 values. Achieved accuracies are close to the values typically provided by standard IRMS and gas chromatographic sampling schemes, respectively. Moreover, no principle problems were met when using the analyzer in combination with a water-air equilibrator setup. Future instrumentation, which will be possibly based on mid-IR instead of near-IR source lasers and thus will benefit from significantly stronger absorptions of vibrational mid-IR transitions, can be expected to provide even better sensitivity.

To ensure the highest possible precision for ambient air measurements, quantitative CO_2 detection was based on absorption peak heights instead of an absorption line integration method. Therefore, care had to be taken when performing measurements in gas matrices with a composition different from that of ambient air. As has been demonstrated in this work, a straightforward spectroscopically based correction procedure can be used in such cases to correct for the corresponding pressure broadening linewidth effects.

Having set the framework for accurate isotope ratio measurements, as a next step, online measurements of surface water $\delta^{13}C(CO_2)$ aboard research vessels are necessary to test CRDS performance in the field. Optimum measurement cycles as well as averaging intervals need to be worked out that finally determine the accessible precision of the instrument. Moreover, these field experiments will show to what extent gas matrix effects need to be taken into account for natural samples and whether it is possible to properly correct for these effects. Corresponding work in these directions is underway.

Appendix

Assuming a known Ar/N_2 ratio set to its ambient value r = 0.01/0.781, it is possible to calculate the O_2 content from the measured Galatry line shape parameter y and the water content xH_2O of the gas mixture. Combining Eq. 8 and xO_2 = $1 - xN_2 - xAr - xH_2O$ yields

$$xO_2 = \frac{(1+r)(y - xH_2O \times y^o_{H_2O}) - (1 - xH_2O)(r y^o_{Ar} + y^o_{N_2})}{(1+r)y^o_{O_2} - r y^o_{Ar} - y^o_{N_2}} \qquad (9)$$

Here, xO_2 corresponds to the mole fraction of O_2 in humid air. y_i^0 values can be obtained from measurements as shown in Fig. 7. For our spectrometer, y_i^0 values have been determined to be 1.64509 (N_2), 1.34393 (O_2), 1.21015 (Ar), 1.5778 (air), 1.9788 (H_2O), and 1.40374 (He). Small deviations from these values can be expected for other spectrometers due to residual baseline fitting errors. From the H_2O measurements shown in the insert of Fig. 7, the precision of the determined y can be estimated to be on the order of ± 0.0015 corresponding to a ±0.5% uncertainty of the calculated absolute O_2 mole fraction. According to the definition of the *relative* supersaturation parameter s for dry air,

$$\frac{xO_2(\text{measured})}{xO_2(\text{air})} = 1 + s \qquad (10)$$

the respective relative supersaturation can thus be determined

to ±2.4% for ambient conditions. Note that the uncertainty of the measured H_2O concentration, which is also affected by the gas matrix effect, can be expected to be small. Assuming a gas matrix effect similar to the one observed for $^{12}CO_2$ (*see* Fig. 6), an H_2O mole fraction error on the order of $\Delta(xH_2O)/xH_2O \approx 1\%$ can be estimated for $s = 0.25$. Assuming a measurement in air with $xH_2O = 0.01$, this 1% error corresponds to an additional uncertainty of the calculated O_2 mole fraction of merely 0.01%.

Although the obtained accuracy for xO_2 is not outstanding, it allows one to measure $\delta^{13}C$ and pCO_2 values of supersaturated surface waters without the need for an additional O_2 sensor. Note that the absolute accuracy of the widely used oxygen optodes, which is typically on the order of < 5% air saturation (Model 4835, AADI), is in fact comparable to our value. In view of the fact that our measurement represents a rather indirect determination of O_2 content, this is a quite surprising result. It again demonstrates the reliability of the high resolution gas phase absorption *cw*-CRDS approach. Of course, the intrinsic precision of optodes is better than the stated absolute uncertainty such that O_2 measurements with higher accuracy can be easily performed by proper referencing to known O_2 concentrations (Tengberg et al. 2006).

References

Berden, G., R. Peeters, and G. Meijer. 2000. Cavity ring-down spectroscopy: Experimental schemes and applications. Int. Rev. Phys. Chem. 19:565-607.

Castrillo, A., M. van Burgel, D. Tedesco, and L. Gianfrani. 2004. First field determination of the $^{13}C/^{12}C$ isotope ratio in volcanic CO_2 by diode-laser spectrometry. Optics Exp. 26:6515-6523 [doi:10.1364/OPEX.12.006515].

Emerson, S. R., and J. I. Hedges. 2008. Chemical oceanography and the marine carbon cycle. Cambridge Univ. Press [doi:10.1017/CBO9780511793202].

Friedrichs, G. 2008. Sensitive absorption methods for quantitative gas phase kinetic measurements. Part 2: Cavity ring-down spectroscopy. Z. Phys. Chem. 222:31-61 [doi:10.1524/zpch.2008.222.1.31].

Galatry, L. 1961. Simultaneous effect of doppler and foreign gas broadening on spectral lines. Phys. Rev. 122:1218-1223 [doi:10.1103/PhysRev.122.1218].

deGroot, P. A. [ed.]. 2004. Handbook of stable isotope analytical techniques, v. 1. Elsevier.

Gruber, N., C. D. Keeling, and N. R. Bates. 2002. Interannual variability in the north Atlantic ocean carbon sink. Science 298:2374-2378 [doi:10.1126/science.1077077].

Haisch, M., P. Hering, P. Schadewald, H. Brösicke, B. Braden, S. Koletzko, and C. Steffen. 1994. Biomedical application of an isotope selective nondispersive infrared spectrometer for $^{13}CO_2$ and $^{12}CO_2$ concentration measurements in breath samples. Isotopes Environ. Health Stud. 30:253-257 [doi:10.1080/00211919408046741].

Hamme, R. C., and S. R. Emerson. 2006. Constraining bubble dynamics and mixing with dissolved gases: implications for productivity measurements by oxygen mass balance. J. Mar. Res. 64:73-95 [doi:10.1357/002224006776412322].

Jäger, F., G. Wagner, H. A. J. Meijer, and E. R. T. Kerstel. 2005. Measuring $\delta^{13}C$ of atmospheric air with non-dispersive infrared spectroscopy. Isotopes Environ. Health Stud. 41:373-378 [doi:10.1080/10256010500384275].

Jost, H. J., A. Castrillo, and H. W. Wilson. 2006. Simultaneous $^{13}C/^{12}C$ and $^{18}O/^{16}O$ isotope ratio measurements on CO_2 based on off-axis integrated cavity output spectroscopy. Isotopes Environ. Health Stud. 42:37-45 [doi:10.1080/10256010500503163].

Keeling, C. D., H. Brix, and N. Gruber. 2004. Seasonal and long-term dynamics of the upper ocean carbon cycle at station ALOHA near Hawaii. Global Biogeochem. Cycles 18:GB4006/1-26.

Kerstel, E. 2004. Isotope ratio infrared spectrometry, p. 759-787. *In* P. A. deGroot [ed.], Handbook of stable isotope analytical techniques. Elsevier.

———, and L. Gianfrani. 2008. Advances in laser-based isotope ratio measurements: Selected applications. Appl. Phys. B 92:439-449 [doi:10.1007/s00340-008-3128-x].

Körtzinger, A., U. Send, D. W. R. Wallace, J. Karstensen, and M. DeGrandpre. 2008. Seasonal cycle of O_2 and pCO_2 in the central Labrador Sea: Atmospheric, biological, and physical implications. Global Biogeochem. Cycles 22:GB1014/1-16.

Kuss, J., W. Roeder, K. Wlost, and M. D. DeGrandpre. 2006. Time-series of surface water CO_2 and oxygen measurements on a platform in the central Arkona Sea (Baltic Sea): Seasonality of uptake and release. Mar. Chem. 101:220-232 [doi:10.1016/j.marchem.2006.03.004].

Lau, S., K. Salffner, and H. G. Löhmannsröben. 2006. Isotopic resolution of carbon monoxide and carbon dioxide by NIR diode laser spectroscopy. Proc SPIE 6189:538-543.

Lüger, H., D. W. R. Wallace, A. Körtzinger, and Y. Nojiri. 2004. The pCO_2 variability in the midlatitude North Atlantic Ocean during a full annual cycle. Global Biogeochem. Cycles 18:GB3023.

———, R. Wanninkhof, D. W. R. Wallace, and A. Körtzinger. 2006. CO_2 fluxes in the sub-tropical and subarctic North Atlantic based on measurements from a volunteer observing ship. J. Geophys. Res. 111:CO6024/1-10.

Mazurenka, M., A. J. Orr-Ewing, R. Peverall, and G. A. D. Ritchie. 2005. Cavity ring-down and cavity enhanced spectroscopy using diode lasers. Annu. Rep. Prog. Chem. C 101:100-142 [doi:10.1039/b408909j].

McIlroy, A., and J. B. Jeffries. 2002. Cavity ringdown spectroscopy for concentration measurements, p. 98-127. *In* K. Kohse-Höinghaus and J. B. Jeffries [eds.], Applied combustion diagnostics. Taylor and Francis.

Mikhailenko, S. N., K. A. Keppler, G. Mellau, S. Klee, B. P. Winnewisser, and V. G. Tyuterev. 2008. Water vapor absorption line intensities in the 1900-6600 cm^{-1} region. J. Quant.

Spectrosc Radiat. Transfer 109:2687-2696 [doi:10.1016/j.jqsrt.2008.07.006].

Mohn, J., R. A. Werner, B. Buchmann, and L. Emmenegger. 2007. High-precision $\delta^{13}CO_2$ analysis by FTIR spectroscopy using a novel calibration strategy. J. Mol. Struct. 834-836:95-101 [doi:10.1016/j.molstruc.2006.09.024].

Mook, W. G. 1986. 13C in atmospheric CO_2. Neth. J. Sea Res. 20:211–223 [doi:10.1016/0077-7579(86)90043-8].

———, J. C. Bommerson, and W. H. Staverman. 1974. Carbon isotope fractionation between dissolved bicarbonate and gaseous carbon dioxide. Earth Planet. Sci. Lett. 22:169-176 [doi:10.1016/0012-821X(74)90078-8].

Nakamichi, S., and others. 2006. Buffer-gas pressure broadening for the (3001)III ← (000) band of CO_2 measured with continuous-wave cavity ring-down spectroscopy. Phys. Chem. Chem. Phys. 8:364-368 [doi:10.1039/b511772k].

Perevalov, B. V., A. Campargue, B. Gao, S. Kassi, S. A. Tashkun, and V. I. Perevalov. 2008a. New CW-CRDS measurements and global modeling of $^{12}C^{16}O_2$ absolute line intensities in the 1.6 μm region. J. Mol. Spectrosc. 252:190-197 [doi:10.1016/j.jms.2008.08.006].

———, T. Deleporte, A. Liu, S. Kassi, A. Campargue, J. V. Auwera, S. A. Tashkun, and V. I. Perevalov. 2008b. Global modeling of $^{13}C^{16}O_2$ absolute line intensities from CW-CRDS and FTS measurements in the 1.6 μm and 2.0 μm regions. J. Quant. Spectrosc. Radiat. Transfer 109:2009-2026 [doi:10.1016/j.jqsrt.2008.02.008].

Quay, P., and J. Stutsman. 2003. Surface layer carbon budget for the subtropical N. Pacific: $\delta^{13}C$ constraints at station ALOHA. Deep Sea Res. I 50:1045-1061 [doi:10.1016/S0967-0637(03)00116-X].

———, R. Sonnerup, J. Stutsman, J. Maurer, A. Körtzinger, X. A. Padin, and C. Robinson. 2007. Anthropogenic CO_2 accumulation rates in the North Atlantic Ocean from changes in the $^{13}C/^{12}C$ of dissolved inorganic carbon. Global Biogeochem. Cycles 21:GB1009/1-15.

———, J. Stutsman, R. A. Feely, and L. W. Juranek. 2009. Net community production rates across the subtropical and equatorial Pacific Ocean estimated from air-sea $\delta^{13}C$ disequilibrium. Global Biogeochem. Cycles 23:GB2006/1-15.

Romanini, D., A. A. Kachanov, N. Sadeghi, and F. Stoeckel. 1997. CW cavity ringdown spectroscopy. Chem. Phys. Lett. 264:316-322 [doi:10.1016/S0009-2614(96)01351-6].

Tagliabue, A., and L. Bopp. 2008. Towards understanding global variability in ocean carbon-13. Global Biogeochem. Cycles 22:GB1025/1-13.

Takahashi, T., J. Olafsson, J. G. Goddard, D. W. Chipman, and S. C. Sutherland. 1993. Seasonal variation of CO_2 and nutrients in the high-latitude surface oceans: a comparative study. Global Biogeochem. Cycles 7:843-878 [doi:10.1029/93GB02263].

Tengberg, A., and others. 2006. Evaluation of a lifetime-based optode to measure oxygen in aquatic systems. Limnol. Oceanogr. Methods 4:7-17.

Wahl, E. H., and others. 2006. Application of cavity ring-down spectroscopy to high precision isotope ratio measurement of $^{13}C/^{12}C$ in carbon dioxide. Isotopes Environ. Health Stud. 42:21-35 [doi:10.1080/10256010500502934].

Watson, A. J., and others. 2009. Tracking the variable North Atlantic Sink for atmospheric CO_2. Science 326:1391-1393 [doi:10.1126/science.1177394].

Zeebe, R. E., and D. Wolf-Gladrow. 2001. CO_2 in seawater: Equilibrium, kinetics, isotopes. Elsevier. Elsevier oceanography series, 65.

———, D. A. Wolf-Gladrow, and H. Jansen. 1999. On the time required to establish chemical and isotopic equilibrium in the carbon dioxide system in seawater. Mar. Chem. 65:135-153 [doi:10.1016/S0304-4203(98)00092-9].

Zhang, J., P. D. Quay, and D. O. Wilbur. 1995. Carbon isotope fractionation during gas-water exchange and dissolution of CO_2. Geochim. Cosmochim. Acta 59:107-114 [doi:10.1016/0016-7037(95)91550-D].

Submitted 18 December 2009
Revised 14 July 2010
Accepted 14 September 2010